

Cavity Heisenberg-spin-chain quantum battery

Fu-Quan Dou ^{*}, Hang Zhou, and Jian-An Sun*College of Physics and Electronic Engineering, Northwest Normal University, Lanzhou 730070, China*

(Received 21 June 2022; accepted 1 September 2022; published 14 September 2022)

We propose a cavity Heisenberg-spin-chain (CHS) quantum battery (QB) with the long-range interactions and investigate its charging process. The performance of the CHS QB is substantially improved compared to the Heisenberg spin chain (HS) QB. When the number of spins $N \gg 1$, the quantum advantage α of the QB's maximum charging power can be obtained, which approximately satisfies the superlinear scaling relation $P_{\max} \propto N^\alpha$. The CHS QB can approach $\alpha = 2$ by optimizing the parameters. We find that the maximum stored energy of the CHS QB has a critical phenomenon. By analyzing the Wigner function, von Neumann entropy, and logarithmic negativity, we demonstrate that entanglement can be a necessary ingredient for QB to store more energy, but not sufficient.

DOI: [10.1103/PhysRevA.106.032212](https://doi.org/10.1103/PhysRevA.106.032212)

I. INTRODUCTION

With the development of quantum science, the potential usefulness of quantum technology in the energy field has attracted a considerable number of authors to introduce and study the “quantum battery (QB),” i.e., a quantum system that stores or supplies energy [1–5]. Different from traditional batteries, the QB usually refers to devices that utilize quantum degrees of freedom to store and transfer energy based on quantum thermodynamics [6,7]. Up to now, considerable attention has been mostly focused on the charging process including the QB's work-extraction capabilities [2,8–23], stable charging [10–12,24–27], self-discharging [23,28], and dissipation charging [11,26,27,29–31]. Alicki and Fannes suggested that “entangling unitary controls,” i.e., unitary operations acting globally on the state of the N quantum cells, lead to better work-extraction capabilities from the QB, when compared to unitary operations acting on each quantum cell separately [1]. Further research uncovered that entanglement generation benefits the speedup of work extraction [17]. Later on, two types of charging schemes, “parallel” and “collective” schemes were proposed [2,14]. During the charging procedure of a QB, there is a “quantum advantage” in the collective charging scheme, that is, when $N \geq 2$, the charging power of the QB is greater than that of the parallel scheme [10,16,28,32–40].

In the quest for such a quantum advantage and potential experimental implementations of QBs, various models have been proposed, which can be mainly divided into two categories: the quantum cavity model, where arrays of N qubits are coupled to a cavity field [8,14,15,18,41–46], and atomic models (two-level atoms, three-level atoms, spin, etc.) [8–14,20,32–35,47–56]. Excitingly, following these theoretical studies, there have been some experimental explorations of QBs [57–63]. The first experimental evidence has been

reported in the Dicke QB system where an organic semiconductor plays the role of an ensemble of two-level systems coupled to a microcavity [57]. Recently, the QBs realized with transmon qutrits [58], Xmon qutrits [59], quantum dots [61], IBM Quantum Platforms [60], star-topology spin systems [62], and QB-enabled Internet-of-Things system [63] have been reported, further testifying to the significant advancements on this topic.

The Heisenberg-spin-chain (HS) model is a statistical mechanical model of spin systems, which plays a crucial role in accounting for the magnetic and thermodynamic natures of many-body systems [64–71]. In recent years, a wide range of work has been done based on the HS model and rich phenomena have been discovered, including the effects of anisotropy parameters and the role of boundary conditions [67,72–85]. In the field of QBs, the HS model has also received considerable attention [9,20,33,48–55]. The spin-spin interactions can yield an advantage in charging power over the noninteracting case, and this advantage can grow super extensively when the interactions are long ranged [33]. The study on dynamics of the HS QB has shown that the defects or impurities can create a larger amount of quenched averaged power in the QB in comparison with the situation where the initial state is prepared without disorder [48]. Furthermore, with the proper tuning of system parameters in the HS QB, an initial state prepared at a finite temperature can generate power in the QB higher than that obtained at zero temperature [48]. An interesting finding is that, after adjusting the magnetic field in the charging, the interacting rotation-time symmetric chargers have the potential to produce a an amount of power higher than that of the corresponding Hermitian chargers [86].

However, previous work on the spin-chain-model QB focused on nearest-neighbor interactions [9,20,33,48–55]. It is well known that the generation of many interesting and exotic physical phenomena relies on the long-range interactions between spins [71]. On the other hand, it has been verified that an N -spin chain coupled to a cavity field can notably enhance

*doufq@nwnu.edu.cn

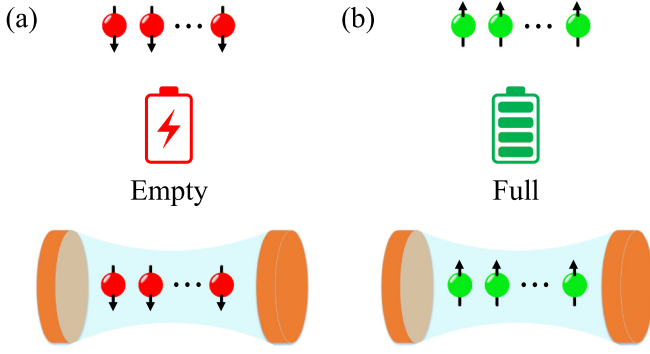


FIG. 1. A sketch of the HS QB and the CHS QB. (a) The state of the HS QB and the CHS QB when they have no energy to output. All the spins are in the ground state, and the battery is empty. (b) The HS QB and the CHS QB are in a fully charged state. All identical spins are all in the spin-up state.

the charging power of a QB [35,41]. Therefore, the following question naturally arises: Under the long-range interactions, how does the cavity Heisenberg-spin-chain (CHS) QB perform compared to the HS QB?

In this work, we propose a CHS QB with long-range interactions and investigate the performance of the CHS QB (including, as well, the HS QB as a comparison). Here the battery consists of N spins displayed in a collective mode during the charging process, and the charger includes the cavity-spin coupling and the spin-spin interaction. We investigate the effect of the cavity on QB's performance. We are concerned with the dependence of the stored energy and the average charging power of the QB on the spin-spin interaction and anisotropy. In addition, we analyze how the number N of the spins influences the maximum stored energy and the maximum charging power. We are also concerned with the quantum advantage of the maximum charging power of the QB. Finally, we show a critical behavior for the maximum stored energy of the CHS QB and introduce the quantum phase transition, the Wigner function, the von Neumann entropy, and the logarithmic negativity to analyze the critical behavior.

This paper is organized as follows. Section II introduces the concept of the CHS QB and the measure to quantify QB's performance. In Sec. III, we give detailed results and analysis of the CHS QB. The critical behavior is dealt with in Sec. IV. Finally, a brief summary is given in Sec. V.

II. QUANTUM SPIN MODEL AS BATTERY

The CHS QB model consists of a single-mode cavity and HS, which are coupled via the exchanges of photons. Figures 1(a) and 1(b) illustrate the initial and charged states of the HS QB and the CHS QB, respectively. The Hamiltonian of the CHS QB can be written as (hereafter, we set $\hbar = 1$)

$$H(t) = H_B + \lambda(t)H_C, \quad (1)$$

TABLE I. Heisenberg model classification.

γ	Δ	Model
$\gamma = \pm 1$	$\Delta = 0$	Ising model [33,52]
$\gamma = 0$	$\Delta = 0$	XX model [49,51,53,86]
$\gamma = 0$	$\Delta = 1$	XXX model [33]
$\gamma = 0$	$\Delta \neq 0$	XXZ model [9,20,33,52,86]
$0 < \gamma < 1$	$\Delta = 0$	XY model [48,50,51,51]
$0 < \gamma < 1$	$\Delta \neq 0$	XYZ model [48]

where

$$H_B = \omega_a \hat{J}_z, \quad (2)$$

$$H_C = \omega_c \hat{a}^\dagger \hat{a} + g_1 \sum_{i=1}^N \hat{\sigma}_i^x (\hat{a}^\dagger + \hat{a}) + \omega_a g_2 \sum_{i<j}^N [(1 + \gamma) \hat{\sigma}_i^x \hat{\sigma}_j^x + (1 - \gamma) \hat{\sigma}_i^y \hat{\sigma}_j^y + \Delta \hat{\sigma}_i^z \hat{\sigma}_j^z]. \quad (3)$$

Here the time-dependent parameter $\lambda(t)$ describes the charging time interval, which we assume to be given by a step function equal to 1 for $t \in [0, T]$ and zero elsewhere. $\hat{\sigma}_i^\alpha$ is the Pauli operators of the i th site. $\hat{J}_\alpha = (\hbar/2) \sum_i^N \hat{\sigma}_i^\alpha$, with $\alpha = x, y, \text{ and } z$. \hat{a} (\hat{a}^\dagger) annihilates (creates) a cavity photon with the cavity field frequency ω_c and the strength of the spin-cavity coupling is given by the dimensionless parameter g_1 , and ω_a is the frequency of spins. γ and Δ are the anisotropy coefficients and N is the number of spins. We focus on the resonance regime, i.e., $\omega_a = \omega_c = 1$, to ensure the maximum energy transfer. The off-resonance case $\omega_a \neq \omega_c$ is not discussed since it is characterized by a less efficient energy transfer between the cavity and the spins.

By introducing the ladder operator $\hat{J}_\pm = \hat{J}_x \pm i\hat{J}_y$, the Hamiltonian H_C can be rewritten as

$$H_C = \omega_c \hat{a}^\dagger \hat{a} + 2g_1 \hat{J}_x (\hat{a}^\dagger + \hat{a}) + \omega_a g_2 \left[\hat{J}_+ \hat{J}_- + \hat{J}_- \hat{J}_+ + \gamma (\hat{J}_+^2 + \hat{J}_-^2) + 2\Delta \hat{J}_z^2 - \frac{N}{2} (2 + \Delta) \right]. \quad (4)$$

By selecting different anisotropy coefficients γ and Δ , the Heisenberg model can be further subdivided into the following categories, and the QBs based on these models have been studied as shown in Table I.

In the usual case, the Heisenberg QB model is charged by an external driving field [9,20,33,48–53]. An energy-charged cavity field in an excited energy state can save as much as an external driving field [41]. However, the effect of the coupling between the spin chain and the cavity on the HS QB has seldom been taken into consideration. Therefore, in our QB model, the XYZ HS is the battery part coupled with a cavity field that transfers energy to charge the QB. Different from the Dicke QB [41], our QB is based on spin chains and takes into account spin-spin interactions.

In our charging protocol, the QB will start charging when the classical parameter $\lambda(t)$ is nonzero. The wave function of the system evolves with time, i.e.,

$$|\Psi(t)\rangle = e^{-iHt/\hbar}|\Psi(0)\rangle, \quad (5)$$

where the $|\Psi(0)\rangle$ is the initial state of the entire system. We consider the charging process of the CHS QB in a closed quantum system. Here, the N spins are prepared in the ground state $|g\rangle$ and coupled to a single-mode cavity in the N photons' Fock-state $|N\rangle$. Thus, the initial state of Eq. (1) is

$$|\Psi(0)\rangle = |N\rangle \otimes \underbrace{|g, g, \dots, g\rangle}_N. \quad (6)$$

At a particular time instant t , the total stored energy by the battery can be defined as

$$E(t) = \langle \Psi(t) | H_B | \Psi(t) \rangle - \langle \Psi(0) | H_B | \Psi(0) \rangle. \quad (7)$$

The corresponding average power for a given time t can be written as $P(t) = E(t)/t$. To maximize the extractable power, it is important to choose a proper time when the evolution should be stopped. Towards this objective, the maximum stored energy E_{\max} (at time t_E) obtained from a given battery can be quantified as

$$E_{\max} \equiv \max_t [E(t)] = E[t_E], \quad (8)$$

and accordingly the maximum power P_{\max} (at time t_P) reads

$$P_{\max} \equiv \max_t [P(t)] = P[t_P]. \quad (9)$$

A convenient basis set for representing the Hamiltonian is $|n, j, m\rangle$, where n indicates the number of photons. With this notation, the initial state in Eq. (2) reads $|\Psi(0)\rangle = |N, N/2, -N/2\rangle$.

The matrix elements of the Hamiltonian H can be evaluated over the basis set $|n, j, m\rangle$ using the following relations for the ladder operator of photons and pseudospin [87–89]:

$$\begin{aligned} \hat{a}^\dagger |n, j, m\rangle &= \sqrt{n+1} |n+1, j, m\rangle, \\ \hat{a} |n, j, m\rangle &= \sqrt{n} |n-1, j, m\rangle, \\ \hat{J}_\pm |n, j, m\rangle &= \sqrt{j(j+1) - m(m \pm 1)} |n, j, m \pm 1\rangle, \end{aligned} \quad (10)$$

while the matrix elements of the CHS Hamiltonian can be found in the Appendix.

We remark that the number of photons is not conserved by the CHS Hamiltonian. It is also not bounded from above; thus, it may take an arbitrarily large integer value. In practice, we need to introduce a cutoff of $N_{\text{ph}} > N$ on the maximum number N_{ph} of photons within our finite-size numerical diagonalization. This choice allows us to select a case scenario of large N values to calculate the stored energy without making any significant difference [41,46]. In this paper, we selecting the maximum number of photons as $N_{\text{ph}} = 4N$. Part of the calculations are coded in PYTHON using the QuTiP library [90].

III. QB'S ENERGY AND CHARGING POWER

In this section, we discuss the charging property of the CHS QB and give some calculation results of HS QB for comparison.

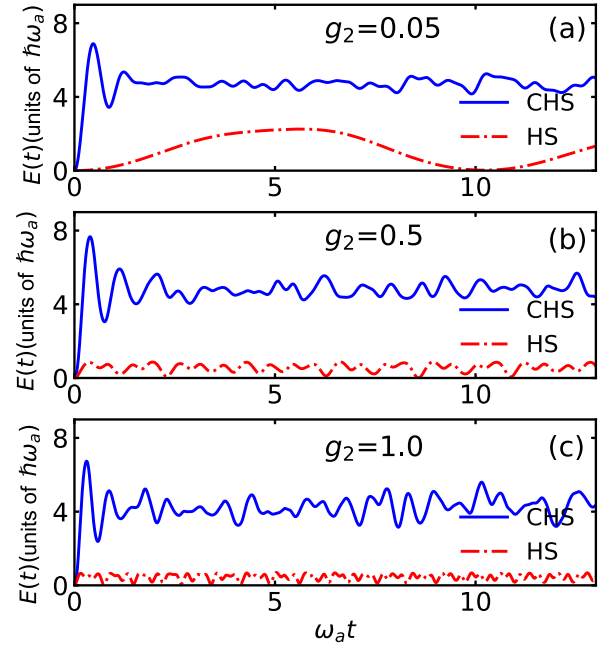


FIG. 2. (a) The dependence of the stored energy $E(t)$ (in units of $\hbar\omega_a$) on $\omega_a t$ for different interaction strengths: (a) $g_2 = 0.05$, (b) $g_2 = 0.5$, and (c) $g_2 = 1.0$. The CHS QB (blue solid line) and the HS QB (red dash-dot line), respectively. In the paper, all plots are under the same setting of $N = 10$, $g_1 = 2$, $\gamma = 0.5$, and $\Delta = 2$, unless mentioned otherwise.

In order to analyze the effect of the cavity on CHS QB, we illustrate the time evolution of energy as shown in Fig. 2. It demonstrates that the CHS QB has better performance than the HS QB. In particular, the CHS QB requires less time to achieve the maximum stored energy because of the presence of the cavity.

We then calculate the maximum stored energy and the maximum charging power of the CHS QB as a function of the anisotropy coefficients and the results are shown in Fig. 3.

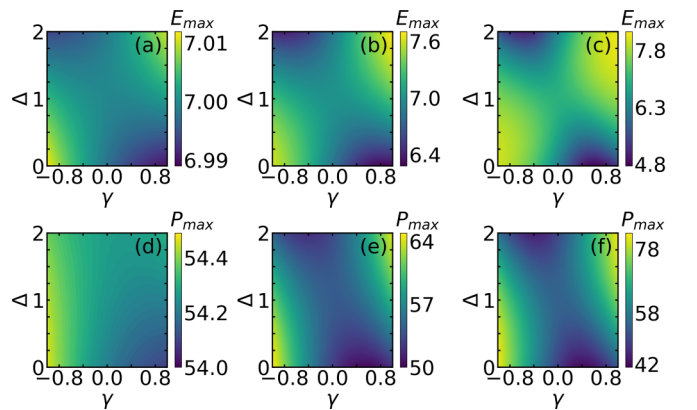


FIG. 3. The contour plots of the CHS QB's maximum stored energy E_{\max} (in units of $\hbar\omega_a$) [panels (a)–(c)] and maximum charging power P_{\max} (in units of $\hbar\omega_a^2$) [panels (d)–(f)] with different values of g_2 . The values of g_2 are as follows: (a) and (d): $g_2 = 0.05$, (b) and (e): $g_2 = 0.5$, and (c) and (f): $g_2 = 1$, respectively. Here, we consider the ranges $\gamma \in [-1, 1]$, $\Delta \in [0, 2]$.

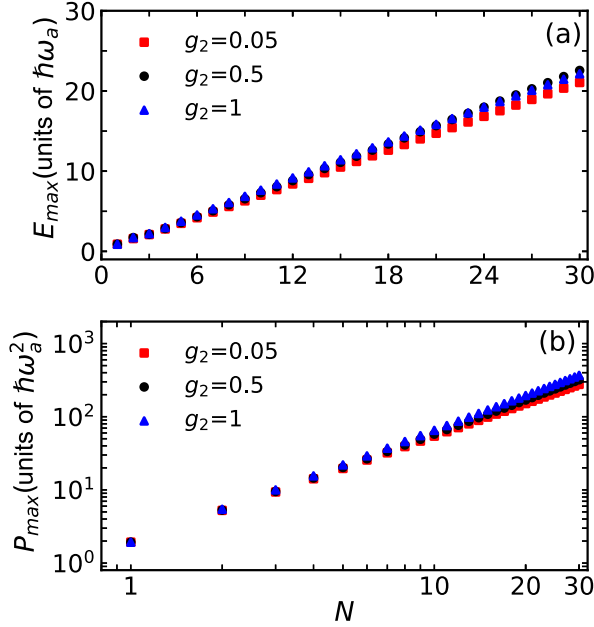


FIG. 4. (a) The maximum stored energy E_{\max} (in units of $\hbar\omega_a$) as a function of N for different values of g_2 . Results for the CHS QB refer to $g_2 = 0.05$ (red circles), $g_2 = 0.5$ (blue triangles), and $g_2 = 1.0$ (red circles). (b) The maximum charging power P_{\max} (in units of $\hbar\omega_a^2$) as a function of N . Color coding and labeling are the same as in panel (a).

The effect of anisotropy on the maximum stored energy and the maximum charging power of the CHS QB is almost negligible for weak spin-spin interaction strength. This effect becomes more prominent with the enhancement of spin-spin interactions. In other words, stronger spin-spin interaction strength can improve the performance of the CHS QB, but also reduces its robustness to anisotropy coefficients. Furthermore, stronger anisotropy can lead to better performance of the CHS QB; i.e., when the exchange interactions in the z and x directions are strong ($\Delta \rightarrow 2$ and $\gamma \rightarrow 1$) or the exchange intensity in the y direction is strong and the z direction is weak ($\Delta \rightarrow 0$ and $\gamma \rightarrow -1$), the CHS QB can obtain greater maximum stored energy and maximum charging power.

The calculation results of both the Dicke QB [41] and the extended Dicke QB [45] show that, for large N , the average charging power scales like $P_{\max} \propto N^{3/2}$ in the single-photon Dicke QB. Therefore, we also expect the existence of a general scaling relation between the charging power of the CHS (or HS) QB and the number N of spins. We assume that the maximum charging power takes the following form:

$$P_{\max} \propto \beta N^\alpha. \quad (11)$$

By taking the logarithm, we use linear fitting to obtain the scaling exponent α :

$$\log_{10}(P_{\max}) = \alpha \log_{10}(N) + \log_{10}(\beta). \quad (12)$$

The scaling exponent α essentially reflects the collective nature of the battery in transferring energy.

We find that maximum stored energy and maximum charging power have a clear correlation with N as it increases in Fig. 4. Under the parameters we take, E_{\max} and P_{\max} satisfy

TABLE II. The scaling exponent α of the maximum charging power for different values of the anisotropy coefficient γ , the cavity-spin coupling strength g_1 , and the spin-spin interaction g_2 . $\Delta = 2$ is fixed.

	$g_1 = 0.1$	$g_1 = 0.5$	$g_1 = 2$	
$\gamma = 0.2$	$g_2 = 0.05$	1.69	1.49	1.43
	$g_2 = 0.5$	0.73	0.87	1.43
	$g_2 = 1$	0.68	0.72	1.37
$\gamma = 0.5$	$g_2 = 0.05$	1.82	1.51	1.53
	$g_2 = 0.5$	0.76	1.47	1.49
	$g_2 = 1$	0.70	0.60	1.50
$\gamma = 0.9$	$g_2 = 0.05$	1.99	1.53	1.43
	$g_2 = 0.5$	1.45	1.69	1.54
	$g_2 = 1$	1.23	1.60	1.59

$E_{\max} \propto N$ and $P_{\max} \propto N^{1.5}$. Similar to the extended Dicke quantum battery [45], the scaling exponent can be even higher by adjusting the parameters appropriately and some results are shown in Table II. These calculations show that the scaling exponent α of the CHS QB can be close to 2 (such as when $g_1 = 0.1$, $g_2 = 0.05$, $\gamma = 0.9$, and $\Delta = 2$). This reveals for large but finite N that P_{\max} of the CHS QB can reach the scaling laws:

$$P_{\max} \propto N^2, \quad (13)$$

which is consistent with the conclusion demonstrated by Ref. [39].

For the CHS QB, when $\omega_c = 0$ and $g_1 = 0$, Eq. (1) corresponds to the HS QB model (the Hamiltonian reads as H_{HS}). Its ground state serves as the possible initial state of the QB. A convenient basis set for representing the Hamiltonian is $|j, m\rangle$, where $j(j+1)$ is the eigenvalue of \hat{J}^2 , and m denotes the eigenvalue of \hat{J}_z . Thus, the HS QB's initial state is $|\Psi_0\rangle = |N/2, -N/2\rangle$ and the matrix elements of the HS Hamiltonian can be evaluated over the basis set $|j, m\rangle$ using the following relations for the ladder operator:

$$\hat{J}_{\pm}|j, m\rangle = \sqrt{j(j+1) - m(m \pm 1)}|j, m \pm 1\rangle. \quad (14)$$

(See the Appendix for more details.)

The results of the maximum stored energy and the maximum charging power of the HS QB as a function of the number of spins N are shown in Fig. 5. The E_{\max} of the HS QB does not show a correlation with N and tends to be chaotic. The maximum charging power of the HS QB does not clearly show regularity, but we can calculate that for different values of g_2 , for sufficiently large values of N , P_{\max} follows the scaling law of Eq. (11): $P_{\max} \propto N^{0.75}$. Similarly, the α values of the HS QB can also be higher by adjusting the system parameters.

The results of the maximum stored energy and the maximum charging power of the HS QB as a function of the anisotropy coefficients are shown in Fig. 6, which shows the spin-spin interaction g_2 will change the dependence of the HS QB on anisotropy parameters and larger g_2 also increases the maximum charging power of the HS QB.

Compared with the QB in Ref. [33] based on the XXZ spin chains, our HS QB also considers the long-range interactions

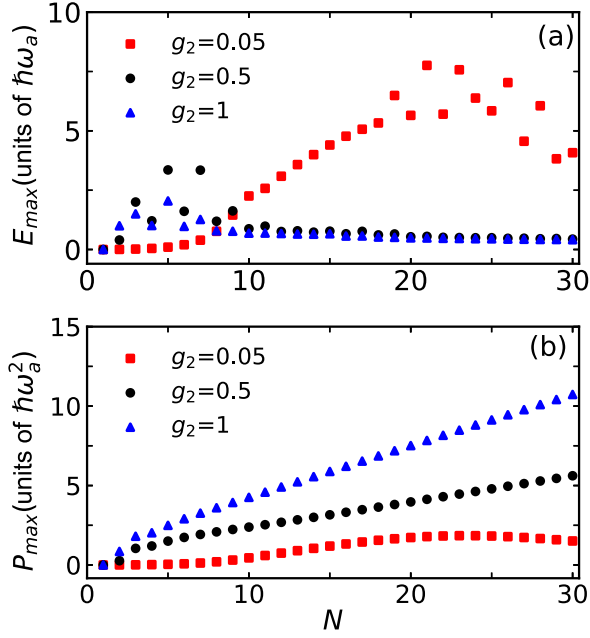


FIG. 5. (a) The maximum stored energy E_{\max} (in units of $\hbar\omega_a$) as a function of N for different values of g_2 . Results for the HS QB refer to $g_2 = 0.05$ (red rectangles), $g_2 = 0.5$ (blue triangles), and $g_2 = 1.0$ (black circles). (b) The maximum charging power P_{\max} (in units of $\hbar\omega_a^2$) as a function of N . Color coding and labeling are the same as in panel (a).

between spins, and the interactions can yield an advantage in charging power. However, different from Ref. [33], where a single many-body battery (with internal interactions) is charged using a local external driving field, in our HS QB based on the XYZ spin chains, the spin-spin interactions are used as the charger rather than as part of the battery. As a result, in Ref. [33], the maximum power obtainable in charging increases as the anisotropy increases and the charging advantage is a mean-field interaction effect that relies on

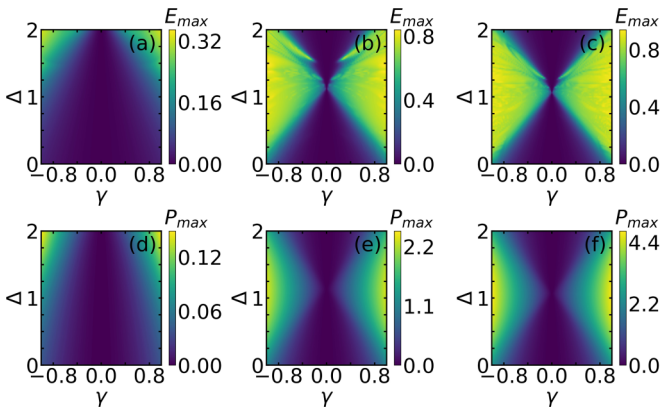


FIG. 6. The contour plots of the HS QB's maximum stored energy E_{\max} (in units of $\hbar\omega_a$) [panels (a)–(c)] and maximum charging power P_{\max} (in units of $\hbar\omega_a^2$) [panels (d)–(f)] with different values of g_2 . The values of g_2 are as follows: (a) and (d): $g_2 = 0.05$, (b) and (e): $g_2 = 0.5$, and (c) and (f): $g_2 = 1$, respectively. Here, we consider the ranges $\gamma \in [-1, 1]$ and $\Delta \in [0, 2]$.

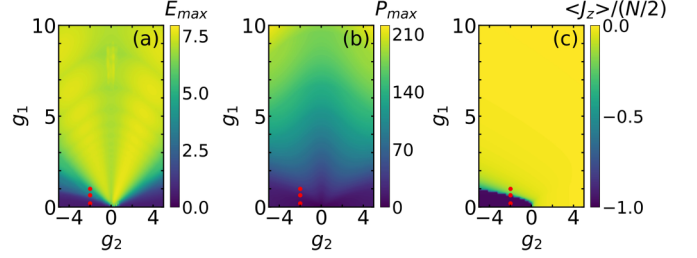


FIG. 7. (a) and (b) Contour plots of the CHS QB's maximum stored energy E_{\max} (in units of $\hbar\omega_a$) and maximum charging power P_{\max} (in units of $\hbar\omega_a^2$) as functions of the cavity-spin coupling strength g_1 and the spin-spin interaction strength g_2 . (c) Phase diagram described by $\langle J_z \rangle / (N/2)$ as functions of the coupling strength g_1 and the interaction strength g_2 . The red dots are three randomly selected points near the critical point.

the interactions being intrinsic to the battery. Nevertheless, in our HS QB, the maximum charging power depends on the anisotropy in each direction and the interaction strength between spins, and the charging advantage is determined by the interplay among them.

IV. ENERGY CRITICAL BEHAVIOR AND ENTANGLEMENT

With the consideration of cavity-spin coupling, a quite natural question follows as to the effects on the charging battery. To do so, we calculated the contour maps of E_{\max} and P_{\max} as a function of the cavity-spin coupling strength g_1 and the spin-spin interaction strength g_2 , as shown in Fig. 7. In regions of weak coupling strength, the spin-spin interaction strength can significantly affect the maximum stored energy of the CHS QB. However, in regions of strong coupling strength, this effect is almost negligible. Particularly, we find that the maximum stored energy of the QB has a critical behavior; i.e., the system exists at a critical point and the maximum stored energy of the QB changes obviously near the critical point.

To clarify such critical behavior, we introduce the quantum phase transition [89,91–95]. Since E_{\max} is measured in the evolution, it is not *a priori* clear that it can identify quantum phase transitions. Figure 7(c) shows the critical curves of the Mott phase [for $|\langle J_z \rangle / (N/2)| = 0$] and the normal phase [for $|\langle J_z \rangle / (N/2)| = 1$]. Correspondingly, at the critical point of the quantum phase transition, the maximum stored energy of the CHS QB changes significantly.

We further introduce the Wigner function, which is a way to visualize quantum states using the phase-space formalism to describe some physical processes and effects [96–102]. We calculated the ground-state cavity Wigner function by randomly selecting three points near the critical point (see Fig. 7) as shown in Fig. 8. For a fixed spin-spin interaction strength, with the enhancement of cavity-spin coupling, the Wigner function splits from one to two peaks at the critical point, which means that the system shows nonclassical properties like coherence and entanglement. However, different from quantum phase transitions, this nonclassical phenomenon does not only occur in the region of spin-spin

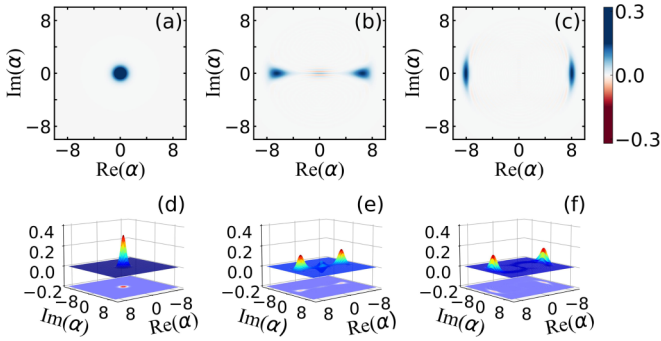


FIG. 8. Wigner function near the critical point (the red dots in Figs. 7 and 9). The values of g_1 and g_2 are as follows: (a) and (d): $(-2, 0.2)$, (b) and (e): $(-2, 0.65)$, and (c) and (f): $(-2, 1.0)$.

attraction; a similar phenomenon is also observed in the region of spin-spin repulsion.

The analysis of the critical behavior and the nonclassical properties of the CHS QB is addressed from the standpoint of the amount of entanglement. We consider the entanglement given by the *von Neumann entropy* [103–105] and the *logarithmic negativity* [106–108]. The former is one of the most standard and simple methods to measure entanglement, and the latter is easy to calculate and provides an upper bound on the distillable entanglement. They are defined by

$$S = -\text{Tr}(\rho_B \log_{10} \rho_B) \quad (15)$$

and

$$E_{\mathcal{N}} = \log_{10} \|\rho^{\text{TB}}\|_1, \quad (16)$$

where $\rho_B = \text{Tr}_A(\rho_{AB})$ is the reduced density matrix of subsystem's battery part. ρ^{TB} denotes the partial transpose of ρ with respect to the battery part. In Fig. 9, we illustrate the relation of S and $E_{\mathcal{N}}$ concerning g_1 and g_2 , showing an obvious critical phenomenon.

For a fixed spin-spin interaction strength, when the cavity-spin coupling strength is less than the critical value, there is no entanglement between the cavity and the spin. Correspondingly, the CHS QB can hardly store energy. As the coupling increases, both the entanglement and the maximum stored energy exhibit critical behavior. The entanglement re-

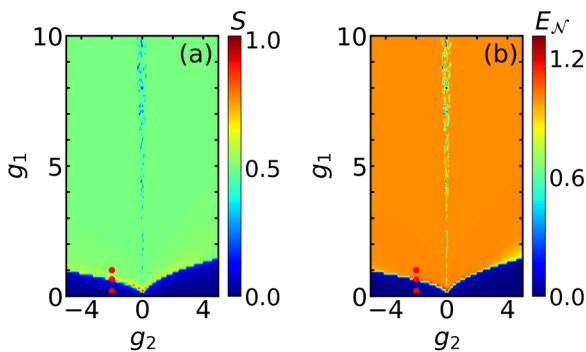


FIG. 9. S and $E_{\mathcal{N}}$ as functions of the cavity-spin coupling strength g_1 and the spin-spin interaction strength g_2 of the CHS QB's ground state. The red dots are three randomly selected points at and near the critical point.

mains stable after attaining a local maximum at the critical point, but the maximum stored energy continues to increase. Moreover, when there is no interaction between the spins, both energy and entanglement appear to have discontinuous behavior, which may be caused by the degeneracy of the ground-state energy level. Such characteristics indicate that entanglement can be necessary for the QB to store more energy, but not sufficient, which is consistent with earlier results [8,48]. Furthermore, our results suggest that some dynamic quantities similar to the maximum stored energy can also carry ground-state information such as quantum phase transitions and entanglement.

V. CONCLUSIONS

We have introduced the concept of the CHS QB, consisting of HS coupling to a single-mode cavity. We have analyzed the influence of parameters such as spin-spin interaction, anisotropy, and cavity-spin coupling on the performance of QBs, including the stored energy and the average charging power. Our results demonstrate that the cavity has a positive effect on the CHS QB in most cases compared to the HS QB. For fixed spin-spin interactions, the cavity-spin coupling strength can increase the maximum stored energy of the QB, but when there is no interaction between spins, the influence of cavity-spin coupling on the maximum stored energy becomes very weak. The maximum charging power shows a pattern similar to that of the maximum stored energy, but the maximum charging power is more sensitive to the cavity-spin coupling strength. The effect of the anisotropy on the maximum stored energy and the maximum charging power of the CHS QB depends on the strength of the spin-spin interactions. To be precise, stronger spin-spin interaction increases the maximum stored energy and the maximum charging power of the CHS QB but reduces their robustness to anisotropy coefficients. We also investigated the effect of the spin number N on the QB's maximum stored energy and found that it increases linearly with N under different spin-spin interaction strengths. In particular, we have obtained the quantum advantage of the QB's maximum charging power, which approximately satisfies the scaling relation $P_{\text{max}} \propto N^\alpha$ where the scaling exponent α varies with the number N of the spins. The quantum advantage of the CHS QB can be approached to $\alpha = 2$ over the HS QB case. Moreover, we find that there is a critical behavior for the maximum stored energy, which is also accompanied by the critical behavior of the quantum phase transitions, the Wigner function, and entanglement, which demonstrates that entanglement can be a necessary ingredient for QB to store more energy, but not sufficient. The physical quantities that detect quantum phase transitions and entanglement are calculated in the ground state, while the maximum stored energy is calculated in the dynamics. Our study shows that even the dynamics quantities can carry ground-state information such as quantum phase transitions and entanglement.

ACKNOWLEDGMENT

This work is supported by the National Natural Science Foundation of China (Grant No. 12075193).

**APPENDIX: MATRIX ELEMENTS
OF THE HAMILTONIAN H AND H_{HS}**

The matrix elements of the Hamiltonian H (or H_{HS}) can be conveniently evaluated over the basis set $|n, j, m\rangle$ (or $|j, m\rangle$), where n indicates the number of photons, $j(j+1)$ is the eigenvalue of \hat{J}^2 , and m denotes the eigenvalue of \hat{J}_z . Notice that, due to the conservation of \hat{J}^2 , one can work in a subspace at fixed $j = N/2$. This leads to

$$\begin{aligned} \left\langle n', \frac{N}{2}, \frac{N}{2} - q' \middle| H \middle| n, \frac{N}{2}, \frac{N}{2} - q \right\rangle = \hbar\omega_c \left\{ \left(n + \frac{N}{2} - q \right) \delta_{q',q} + g_1 \left[f_{n, \frac{N}{2}, \frac{N}{2} - q}^{(1)} \delta_{n', n+1} \delta_{q', q+1} + f_{n, \frac{N}{2}, \frac{N}{2} - q}^{(2)} \delta_{n', n+1} \delta_{q', q-1} \right. \right. \\ \left. \left. + f_{n, \frac{N}{2}, \frac{N}{2} - q}^{(3)} \delta_{n', n-1} \delta_{q', q+1} + f_{n, \frac{N}{2}, \frac{N}{2} - q}^{(4)} \delta_{n', n-1} \delta_{q', q-1} \right] + g_2 \left[f_{n, \frac{N}{2}, \frac{N}{2} - q}^{(5)} \delta_{q', q} + f_{n, \frac{N}{2}, \frac{N}{2} - q}^{(6)} \delta_{q', q} \right. \right. \\ \left. \left. + \gamma \left(f_{n, \frac{N}{2}, \frac{N}{2} - q}^{(7)} \delta_{q'-2, q} + f_{n, \frac{N}{2}, \frac{N}{2} - q}^{(8)} \delta_{q'+2, q} \right) + 2\Delta \left(\frac{N}{2} - q \right)^2 \delta_{q', q} - \frac{N}{2} (2 + \Delta) \right] \right\}, \quad (\text{A1}) \end{aligned}$$

with

$$\begin{aligned} f_{k, j, m}^{(1)} &= \sqrt{(k+1)[j(j+1) - m(m-1)]}, \\ f_{k, j, m}^{(2)} &= \sqrt{(k+1)[j(j+1) - m(m+1)]}, \\ f_{k, j, m}^{(3)} &= \sqrt{k[j(j+1) - m(m-1)]}, \\ f_{k, j, m}^{(4)} &= \sqrt{k[j(j+1) - m(m+1)]}, \\ f_{k, j, m}^{(5)} &= j(j+1) - m(m-1), \\ f_{k, j, m}^{(6)} &= j(j+1) - m(m+1), \\ f_{k, j, m}^{(7)} &= \sqrt{[j(j+1) - (m+1)(m+2)][j(j+1) - m(m+1)]}, \\ f_{k, j, m}^{(8)} &= \sqrt{[j(j+1) - (m-1)(m-2)][j(j+1) - m(m-1)]}, \end{aligned} \quad (\text{A2})$$

and

$$\begin{aligned} \left\langle \frac{N}{2}, \frac{N}{2} - q' \middle| H_{\text{HS}} \middle| \frac{N}{2}, \frac{N}{2} - q \right\rangle = \hbar\omega_a \left\{ \left(\frac{N}{2} - q \right) \delta_{q', q} + g_2 \left[f_{\frac{N}{2}, \frac{N}{2} - q}^{(1)} \delta_{q', q} + f_{\frac{N}{2}, \frac{N}{2} - q}^{(2)} \delta_{q', q} \right. \right. \\ \left. \left. + \gamma \left(f_{\frac{N}{2}, \frac{N}{2} - q}^{(3)} \delta_{q'-2, q} + f_{\frac{N}{2}, \frac{N}{2} - q}^{(4)} \delta_{q'+2, q} \right) + 2\Delta \left(\frac{N}{2} - q \right)^2 \delta_{q', q} - \frac{N}{2} (2 + \Delta) \right] \right\}, \quad (\text{A3}) \end{aligned}$$

with

$$\begin{aligned} f_{j, m}^{(1)} &= j(j+1) - m(m-1), \\ f_{j, m}^{(2)} &= j(j+1) - m(m+1), \\ f_{j, m}^{(3)} &= \sqrt{[j(j+1) - (m+1)(m+2)][j(j+1) - m(m+1)]}, \\ f_{j, m}^{(4)} &= \sqrt{[j(j+1) - (m-1)(m-2)][j(j+1) - m(m-1)]}. \end{aligned} \quad (\text{A4})$$

-
- [1] R. Alicki and M. Fannes, *Phys. Rev. E* **87**, 042123 (2013).
[2] F. Campaioli, F. A. Pollock, F. C. Binder, L. Céleri, J. Goold, S. Vinjanampathy, and K. Modi, *Phys. Rev. Lett.* **118**, 150601 (2017).
[3] S. Bhattacharjee and A. Dutta, *Eur. Phys. J. B* **94**, 239 (2021).
[4] W. Niedenzu, V. Mukherjee, A. Ghosh, A. G. Kofman, and G. Kurizki, *Nat. Commun.* **9**, 165 (2018).
[5] G. L. Giorgi and S. Campbell, *J. Phys. B: At., Mol. Opt. Phys.* **48**, 035501 (2015).
[6] J. Q. Quach and W. J. Munro, *Phys. Rev. Applied* **14**, 024092 (2020).
[7] P. Skrzypczyk, A. J. Short, and S. Popescu, *Nat. Commun.* **5**, 4185 (2014).
[8] F. Campaioli, F. A. Pollock, and S. Vinjanampathy, Quantum batteries, in *Thermodynamics in the Quantum Regime: Fundamental Aspects and New Directions*, edited by F. Binder, L. A. Correa, C. Gogolin, J. Anders, and G. Adesso (Springer International, Cham, 2018), pp. 207–225.
[9] H.-L. Shi, S. Ding, Q.-K. Wan, X.-H. Wang, and W.-L. Yang, [arXiv:2205.11080](https://arxiv.org/abs/2205.11080).
[10] J. Chen, L. Zhan, L. Shao, X. Zhang, Y. Zhang, and X. Wang, *Ann. Phys.* **532**, 1900487 (2020).

- [11] D. Rosa, D. Rossini, G. M. Andolina, M. Polini, and M. Carrega, *J. High Energy Phys.* **11** (2020) 067.
- [12] J. Monsel, M. Fellous-Asiani, B. Huard, and A. Auffèves, *Phys. Rev. Lett.* **124**, 130601 (2020).
- [13] D. Rossini, G. M. Andolina, D. Rosa, M. Carrega, and M. Polini, *Phys. Rev. Lett.* **125**, 236402 (2020).
- [14] F. C. Binder, S. Vinjanampathy, K. Modi, and J. Goold, *New J. Phys.* **17**, 075015 (2015).
- [15] L. Fusco, M. Paternostro, and G. De Chiara, *Phys. Rev. E* **94**, 052122 (2016).
- [16] K. Sen and U. Sen, *Phys. Rev. A* **104**, L030402 (2021).
- [17] K. V. Hovhannisyán, M. Perarnau-Llobet, M. Huber, and A. Acín, *Phys. Rev. Lett.* **111**, 240401 (2013).
- [18] G. M. Andolina, M. Keck, A. Mari, M. Campisi, V. Giovannetti, and M. Polini, *Phys. Rev. Lett.* **122**, 047702 (2019).
- [19] N. Friis and M. Huber, *Quantum* **2**, 61 (2018).
- [20] F. H. Kamin, F. T. Tabesh, S. Salimi, and A. C. Santos, *Phys. Rev. E* **102**, 052109 (2020).
- [21] F. Caravelli, G. Coulter-De Wit, L. P. García-Pintos, and A. Hamma, *Phys. Rev. Research* **2**, 023095 (2020).
- [22] L. P. García-Pintos, A. Hamma, and A. del Campo, *Phys. Rev. Lett.* **125**, 040601 (2020).
- [23] F. Q. Dou, Y. J. Wang, and J. A. Sun, *Europhys. Lett.* **131**, 43001 (2020).
- [24] A. C. Santos, B. Cakmak, S. Campbell, and N. T. Zinner, *Phys. Rev. E* **100**, 032107 (2019).
- [25] F. Q. Dou, Y. J. Wang, and J. A. Sun, *Front. Phys.* **17**, 31503 (2022).
- [26] A. C. Santos, A. Saguia, and M. S. Sarandy, *Phys. Rev. E* **101**, 062114 (2020).
- [27] F. H. Kamin, F. T. Tabesh, S. Salimi, F. Kheirandish, and A. C. Santos, *New J. Phys.* **22**, 083007 (2020).
- [28] A. C. Santos, *Phys. Rev. E* **103**, 042118 (2021).
- [29] M. T. Mitchison, J. Goold, and J. Prior, *Quantum* **5**, 500 (2021).
- [30] K. V. Hovhannisyán, F. Barra, and A. Imparato, *Phys. Rev. Research* **2**, 033413 (2020).
- [31] F. T. Tabesh, F. H. Kamin, and S. Salimi, *Phys. Rev. A* **102**, 052223 (2020).
- [32] Y.-Y. Zhang, T.-R. Yang, L. Fu, and X. Wang, *Phys. Rev. E* **99**, 052106 (2019).
- [33] T. P. Le, J. Levinsen, K. Modi, M. M. Parish, and F. A. Pollock, *Phys. Rev. A* **97**, 022106 (2018).
- [34] S. Julià-Farré, T. Salamon, A. Riera, M. N. Bera, and M. Lewenstein, *Phys. Rev. Research* **2**, 023113 (2020).
- [35] G. M. Andolina, M. Keck, A. Mari, V. Giovannetti, and M. Polini, *Phys. Rev. B* **99**, 205437 (2019).
- [36] W. Chang, T.-R. Yang, H. Dong, L. Fu, X. Wang, and Y.-Y. Zhang, *New J. Phys.* **23**, 103026 (2021).
- [37] L. Peng, W. B. He, S. Chesi, H. Q. Lin, and X. W. Guan, *Phys. Rev. A* **103**, 052220 (2021).
- [38] F. Pirmoradian and K. Mølmer, *Phys. Rev. A* **100**, 043833 (2019).
- [39] J. Gyhm, D. Šafránek, and D. Rosa, *Phys. Rev. Lett.* **128**, 140501 (2022).
- [40] J. Kim, J. Murugan, J. Olle, and D. Rosa, *Phys. Rev. A* **105**, L010201 (2022).
- [41] D. Ferraro, M. Campisi, G. M. Andolina, V. Pellegrini, and M. Polini, *Phys. Rev. Lett.* **120**, 117702 (2018).
- [42] G. M. Andolina, D. Farina, A. Mari, V. Pellegrini, V. Giovannetti, and M. Polini, *Phys. Rev. B* **98**, 205423 (2018).
- [43] D. Farina, G. M. Andolina, A. Mari, M. Polini, and V. Giovannetti, *Phys. Rev. B* **99**, 035421 (2019).
- [44] X. Zhang and M. blaauboer, [arXiv:1812.10139](https://arxiv.org/abs/1812.10139).
- [45] F.-Q. Dou, Y.-Q. Lu, Y.-J. Wang, and J.-A. Sun, *Phys. Rev. B* **105**, 115405 (2022).
- [46] A. Crescente, M. Carrega, M. Sassetti, and D. Ferraro, *Phys. Rev. B* **102**, 245407 (2020).
- [47] J.-X. Liu, H.-L. Shi, Y.-H. Shi, X.-H. Wang, and W.-L. Yang, *Phys. Rev. B* **104**, 245418 (2021).
- [48] S. Ghosh, T. Chanda, and A. Sen(De), *Phys. Rev. A* **101**, 032115 (2020).
- [49] S. Zakavati, F. T. Tabesh, and S. Salimi, *Phys. Rev. E* **104**, 054117 (2021).
- [50] Y. Huangfu and J. Jing, *Phys. Rev. E* **104**, 024129 (2021).
- [51] S. Ghosh and A. Sen(De), *Phys. Rev. A* **105**, 022628 (2022).
- [52] D. Rossini, G. M. Andolina, and M. Polini, *Phys. Rev. B* **100**, 115142 (2019).
- [53] M. B. Arjmandi, H. Mohammadi, and A. C. Santos, *Phys. Rev. E* **105**, 054115 (2022).
- [54] F. Zhao, F.-Q. Dou, and Q. Zhao, *Phys. Rev. Research* **4**, 013172 (2022).
- [55] F. Zhao, F.-Q. Dou, and Q. Zhao, *Phys. Rev. A* **103**, 033715 (2021).
- [56] F.-Q. Dou, Y.-J. Wang, and J.-A. Sun, [arXiv:2208.04831](https://arxiv.org/abs/2208.04831).
- [57] J. Q. Quach, K. E. McGhee, L. Ganzer, D. M. Rouse, B. W. Lovett, E. M. Gauger, J. Keeling, G. Cerullo, D. G. Lidzey, and T. Virgili, *Sci. Adv.* **8**, eabk3160 (2022).
- [58] C.-K. Hu, J. Qiu, P. J. P. Souza, J. Yuan, Y. Zhou, L. Zhang, J. Chu, X. Pan, L. Hu, J. Li, Y. Xu, Y. Zhong, S. Liu, F. Yan, D. Tan, R. Bachelard, C. J. Villas-Boas, A. C. Santos, and D. Yu, *Quantum Sci. Technol.* **7**, 045018 (2022).
- [59] R.-H. Zheng, W. Ning, Z.-B. Yang, Y. Xia, and S.-B. Zheng, *New J. Phys.* **24**, 063031 (2022).
- [60] G. Gemme, M. Grossi, D. Ferraro, S. Vallecorsa, and M. Sassetti, *Batteries* **8**, 43 (2022).
- [61] I. Wenniger, S. Thomas, M. Maffei, S. Wein, M. Pont, A. Harouri, A. Lemaître, I. Sagnes, N. Somaschi, A. Auffèves *et al.*, [arXiv:2202.01109](https://arxiv.org/abs/2202.01109).
- [62] J. Joshi and T. Mahesh, [arXiv:2112.15437](https://arxiv.org/abs/2112.15437).
- [63] S. Gautam, S. Solanki, S. K. Sharma, S. Chatzinotas, and B. Ottersten, *Sensors* **22**, 5385 (2022).
- [64] C. F. Lee and N. F. Johnson, *Phys. Rev. A* **70**, 052322 (2004).
- [65] X. Peng, J. Du, and D. Suter, *Phys. Rev. A* **71**, 012307 (2005).
- [66] M. Bortz, M. Karbach, I. Schneider, and S. Eggert, *Phys. Rev. B* **79**, 245414 (2009).
- [67] F. L. Pratt, S. J. Blundell, T. Lancaster, C. Baines, and S. Takagi, *Phys. Rev. Lett.* **96**, 247203 (2006).
- [68] R. G. Pereira, J. Sirker, J.-S. Caux, R. Hagemans, J. M. Maillet, S. R. White, and I. Affleck, *Phys. Rev. Lett.* **96**, 257202 (2006).
- [69] M. Kohno, *Phys. Rev. Lett.* **102**, 037203 (2009).
- [70] S.-S. Gong and G. Su, *Phys. Rev. A* **80**, 012323 (2009).
- [71] Z.-X. Chen, Z.-W. Zhou, X. Zhou, X.-F. Zhou, and G.-C. Guo, *Phys. Rev. A* **81**, 022303 (2010).
- [72] K. H. Höglund and A. W. Sandvik, *Phys. Rev. Lett.* **99**, 027205 (2007).
- [73] A. J. A. James, W. D. Goetze, and F. H. L. Essler, *Phys. Rev. B* **79**, 214408 (2009).

- [74] M. B. Stone, D. H. Reich, C. Broholm, K. Lefmann, C. Rischel, C. P. Landee, and M. M. Turnbull, *Phys. Rev. Lett.* **91**, 037205 (2003).
- [75] T. Stauber and F. Guinea, *Phys. Rev. A* **70**, 022313 (2004).
- [76] A. Hamma, R. Ionicioiu, and P. Zanardi, *Phys. Rev. A* **71**, 022315 (2005).
- [77] S. Bose, B.-Q. Jin, and V. E. Korepin, *Phys. Rev. A* **72**, 022345 (2005).
- [78] M. Asoudeh and V. Karimipour, *Phys. Rev. A* **71**, 022308 (2005).
- [79] G.-F. Zhang and S.-S. Li, *Phys. Rev. A* **72**, 034302 (2005).
- [80] X.-Y. Ge and M. Wadati, *Phys. Rev. A* **72**, 052101 (2005).
- [81] Z. Huang and S. Kais, *Phys. Rev. A* **73**, 022339 (2006).
- [82] T. Boness, S. Bose, and T. S. Monteiro, *Phys. Rev. Lett.* **96**, 187201 (2006).
- [83] F. Kheirandish, S. J. Akhtarshenas, and H. Mohammadi, *Phys. Rev. A* **77**, 042309 (2008).
- [84] R. H. Crooks and D. V. Khveshchenko, *Phys. Rev. A* **77**, 062305 (2008).
- [85] J. Doukas and L. C. L. Hollenberg, *Phys. Rev. A* **79**, 052109 (2009).
- [86] T. K. Konar, L. G. C. Lakkaraju, and A. S. De, [arXiv:2203.09497](https://arxiv.org/abs/2203.09497).
- [87] M. A. Bastarrachea-Magnani and J. G. Hirsch, *Rev. Mex. Fis. S* **57**, 69 (2011).
- [88] E. Romera, R. del Real, and M. Calixto, *Phys. Rev. A* **85**, 053831 (2012).
- [89] C. Emary and T. Brandes, *Phys. Rev. E* **67**, 066203 (2003).
- [90] J. Johansson, P. Nation, and F. Nori, *Comput. Phys. Commun.* **184**, 1234 (2013).
- [91] G. Chen, X. Wang, J.-Q. Liang, and Z. D. Wang, *Phys. Rev. A* **78**, 023634 (2008).
- [92] G. Chen, D. Zhao, and Z. Chen, *J. Phys. B: At. Mol. Opt. Phys.* **39**, 3315 (2006).
- [93] K. Baumann, C. Guerlin, F. Brennecke, and T. Esslinger, *Nature (London)* **464**, 1301 (2010).
- [94] S.-C. Li, H.-L. Liu, and X.-Y. Zhao, *Eur. Phys. J. D* **67**, 250 (2013).
- [95] S.-C. Li, L.-B. Fu, and J. Liu, *Phys. Rev. A* **84**, 053610 (2011).
- [96] E. Wigner, *Phys. Rev.* **40**, 749 (1932).
- [97] M. Hillery, R. O’Connell, M. Scully, and E. Wigner, *Phys. Rep.* **106**, 121 (1984).
- [98] E. P. Wigner, in *Part I: Physical Chemistry. Part II: Solid State Physics*, edited by A. S. Wightman (Springer, Berlin, 1997), pp. 110–120.
- [99] Y. S. Kim and E. P. Wigner, *Am. J. Phys.* **58**, 439 (1990).
- [100] D. Kohen, C. C. Marston, and D. J. Tannor, *J. Chem. Phys.* **107**, 5236 (1997).
- [101] D. Querlioz and P. Dollfus, *The Wigner Monte Carlo Method for Nanoelectronic Devices: A Particle Description of Quantum Transport and Decoherence* (Wiley & Sons, Hoboken, NJ, 2013).
- [102] J. Weinbub and D. K. Ferry, *Appl. Phys. Rev.* **5**, 041104 (2018).
- [103] W. K. Wootters, *Phys. Rev. Lett.* **80**, 2245 (1998).
- [104] C. H. Bennett, H. J. Bernstein, S. Popescu, and B. Schumacher, *Phys. Rev. A* **53**, 2046 (1996).
- [105] L. Amico, R. Fazio, A. Osterloh, and V. Vedral, *Rev. Mod. Phys.* **80**, 517 (2008).
- [106] M. B. Plenio, *Phys. Rev. Lett.* **95**, 090503 (2005).
- [107] G. Vidal and R. F. Werner, *Phys. Rev. A* **65**, 032314 (2002).
- [108] M. Horodecki, P. Horodecki, and R. Horodecki, *Phys. Rev. Lett.* **84**, 4260 (2000).